Optical Materials 122 (2021) 111653

Contents lists available at ScienceDirect

Optical Materials

journal homepage: www.elsevier.com/locate/optmat

Research Article

Tailoring the properties of tin dioxide thin films by spray pyrolysis technique

Ebitha Eqbal [a,b], E.I. Anila [b,c,*]

[a] Department of Basic Sciences and Humanities, KMEA Engineering College, Edathala, Aluva, 683561, Kerala, India
[b] Optoelectronic and Nanomaterials' Research Laboratory, Department of Physics, Union Christian College, Aluva, 683102, Kerala, India
[c] Department of Physics and Electronics, CHRIST (Deemed to Be University), Bengaluru, 560029, India

ARTICLE INFO

Keywords:
Tin dioxide
Photoluminescence
Texture coefficient
Dislocation density
Grain size

ABSTRACT

Nanostructured transparent conducting SnO_2 thin films have been grown on glass substrates via an environmentally benign chemical route viz spray pyrolysis. All samples were grown for various concentrations of precursor solution with the substrate kept at 350 °C maintaining a spray rate of 10 mL/min. The characterizations revealed orthorhombic crystal structure with preferential growth in (112) plane for all samples. Ellipsometric analysis confirmed the good quality of the films. The sample prepared at 0.2 M concentration of precursor solution showed average transmission of 60% in the visible region with maximum conductivity of 24.86 S/cm. As synthesized samples exhibited overall Photoluminescence (PL) emission colours of green, greenish white and bluish white depending on the intensities of excitonic and oxygen vacancy defect level emissions.

1. Introduction

Tin dioxide (SnO_2) is an n-type semiconducting material with tetragonal rutile structure having a wide band gap of 3.6–4.0 eV [1,2]. The studies on the transparent conducting oxide thin films are significant in the world of semiconducting materials. The vital features of SnO_2 nanostructured thin films include its nontoxicity, high optical transmittance, better electrical conductivity, good piezoelectric behaviour, consistency, stable to heat and not the least its low cost [3–5]. SnO_2 has wide variety of applications in gas sensor devices [6], transistors [7], solar cells [8], optoelectronic devices [9] etc. Literature survey shows that tin oxide thin films could be synthesized by various chemical and physical techniques such as sol-gel method [10], chemical bath deposition [11], spin coating [12], electron beam evaporation [13], PLD [14], sputtering [15], spray pyrolysis [16] etc.

In the present work, SnO_2 thin films are deposited for different molarities of precursor solution via an environmentally benign chemical route viz spray pyrolysis and tailored their structural, optical and electrical properties.

2. Experimental

The AR grade tin chloride dihydrate ($SnCl_2.2H_2O$) was liquified in distilled water to get 0.05 M, 0.15 M, 0.2 M and 0.3 M concentration of precursor solutions. For removing any precipitate in solution, few drops of concentrated hydrochloric acid was added. Then the mixture was vigorously stirred at 60 °C for about 1 h. Pre cleaned and ultrasonically cleaned substrates were placed on the substrate holder of the spray equipment and sufficient heating was given to obtain even films. The spray parameters were optimised as 350 °C, 10 mL/min, 0.2 kg/cm^2 and 15 cm for substrate temperature, spray rate, carrier gas pressure and source substrate distance respectively.

The glass slides were taken immediately after the spray process and allowed to cool to room temperature. This resulted in the formation of uniform, well adherent and transparent SnO_2 thin films.

Structural parameters like average grain size, dislocation density, lattice strain, crystallite size etc. have been analysed using the X-ray diffraction plots (XRD) recorded on a Rigaku D-Max Geigerflex X-ray diffractometer using Cu-K_α radiation source of wavelength 1.5418 Å for 2θ values from 20° to 80° at room temperature. The surface morphology of the as grown films was studied using JEOL JSM 7600F field emission scanning electron microscope. The thickness of the films was measured by Ellipsometry technique using Woollan USA.

The optical characterization of SnO_2 thin film samples were carried out by using Shimadzu UV–Vis spectrophotometer UV 1800. PL characterizations of the samples were done using Fluoromax-4

* Corresponding author. Optoelectronic and Nanomaterials' Research Laboratory, Department of Physics, Union Christian College, Aluva, 683102, Kerala, India.
E-mail address: anila.ei@christuniversity.in (E.I. Anila).

https://doi.org/10.1016/j.optmat.2021.111653
Received 18 August 2021; Received in revised form 27 September 2021; Accepted 2 October 2021
Available online 12 October 2021

Spectrofluorometer. Hall effect measurements using ECOPIA HMS-5000 in Vander Pauw configuration were used to tailor the electrical properties of as grown samples. Illumination on the as prepared samples was provided by a Halogen Reflector lamp (300W/82V) for photoconductivity spectrum measurements and the photocurrent was continuously recorded using a 2450 Keithley Source meter.

3. Results and discussion

3.1. Structural analysis

Fig. 1(a) represents the XRD spectra of SnO_2 thin films in which the major diffraction peaks correspond to (112), (006), (122), (188), (133) and (312) planes of orthorhombic phase in agreement with the standard JCPDS file no: 78–1063. XRD peak intensity increases with increase in concentration of precursor solution which is due to increase in crystallinity of the sample. A slight variation in peak width can also be observed due to change in grain size and lattice strain.

Scherrer's formula provides the average grain size of the samples using the equation [17],

$$D = \frac{0.9\ \lambda}{\beta\ cos\ \theta} \tag{1}$$

where θ is the glancing angle, λ is the wavelength of X-ray radiations and β is the full width at half maximum to the diffraction peak. The dislocation density (δ) which measures the length of dislocation lines per unit volume (lines/m^2) are calculated using the standard relation [17].

$$\text{Dislocationdensity}(\delta) = 1/D^2 \tag{2}$$

The diffraction line broadening caused by the strain and reduced grain size was analysed using the Williamson–Hall (W–H) method. The basic relation used for the calculation of lattice strain and crystallite size [18] by this method is,

$$\beta\ cos\ \theta\ =\ 0.9\ \lambda/D + 2\xi sin\theta \tag{3}$$

Here ξ corresponds to lattice strain. The average grain size evaluated from Scherrer's formula and W–H plot, dislocation density and lattice strain of pristine SnO_2 samples are tabulated in Table 1.

At low precursor concentrations, incorporation of deposited atoms to the neighbouring grains is less and they form small nuclei and clusters. Grain size increases with increasing precursor concentration due to the increased number of clusters and coalescence of small grains. Increase in thin film thickness (Table .3) also favours the growth of grains. Dislocation density shows a decreasing trend with increase in precursor concentration. Lattice strain shows a fluctuating behaviour. It is observed that, 0.05 M and 0.15 M SnO_2 thin films show lattice elongation whereas 0.2 and 0.3 M SnO_2 thin films show lattice compression.

The preferential growth of polycrystalline thin films for each peak can be investigated from the reflection intensity by calculating the texture coefficient [TC (hkl)]. TC (hkl) for the plane is calculated using the following equation [19].

$$TC(hkl) = \frac{I(hkl)}{\frac{1}{N}\Sigma I(hkl)} \tag{4}$$

where TC (hkl) is the texture coefficient of the hkl plane, I(hkl) is the intensity of each plane and N is the number of reflections. Table .2 shows Texture coefficient of each (hkl) plane. The deviation of the texture coefficient from the unity indicates the preferred orientation of the growth. The larger of texture coefficient deviates from unity, the higher will be the preferred orientation of a film. It is clear that (112) has high preferred orientation for all the samples.

Table 1
Crystallite size, dislocation density and lattice strain of SnO_2 thin films for different molarities.

Molarity (M)	Grain size (D) (nm)		Dislocation Density (x 10^{15}) (lines/m^2)	Lattice Strain (arb.units)
	from Eq. (1)	from Fig. 1(b)		
0.05	16.02	17.14	3.89	0.07
0.15	16.18	16.38	3.81	0.09
0.2	20.53	20.10	2.37	−0.48
0.3	20.88	20.74	2.29	−0.05

3.2. Morphological analysis

The morphology of as deposited samples is depicted in Fig. 2. SnO_2 thin film produced with 0.05 M precursor exhibits fine particles on the surface. When the precursor molarity becomes 0.15, the particles grow in size with irregular shape and for higher molarities the particles look like rice grains and they are irregularly distributed and densely packed over the surface. It is found that the grain size increases with molarity and 0.2 M sample has maximum surface smoothness.

3.3. Ellipsometric analysis

The thickness, roughness, refractive index and extinction coefficient

Table 2
Texture coefficient of each (hkl) plane.

(hkl)	TC of Sample1 (0.05 M)	TC of Sample 2 (0.15 M)	TC of Sample 3 (0.2 M)	TC of Sample4 (0.3 M)
(112)	1.71	1.66	1.41	1.66
(006)	1.04	1.10	1.05	1.09
(122)	0.4954	0.4948	0.6977	0.5406
(118)	0.7476	0.7339	0.8260	0.6984

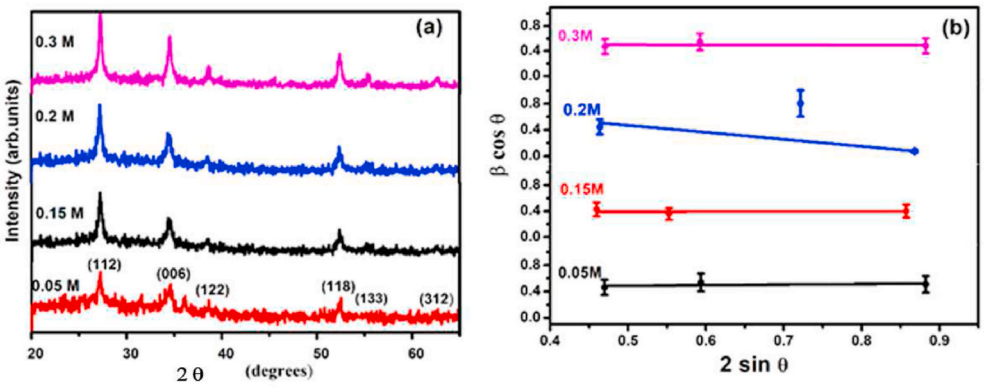

Fig. 1. (a) XRD spectrum and (b) W–H plot of the as grown samples.

Table 3
Ellipsometric analysis of SnO_2 thin films for different molarities.

Molarity (M)	Thickness (nm)	Roughness (nm)	Mean Square Error	Refractive index (n)	Extinction Coefficient (k)
0.05	70	3.56	5.14	1.7301	0.2741
0.15	100	3.22	4.87	1.7367	0.1334
0.2	133	3.12	3.99	1.7412	0.1567
0.3	150	3.63	4.57	1.7619	0.1159

of the thin films are determined via ellipsometric analysis. If mean square error (MSE) is less than 10, it can be adjudged as good quality films and in the present study, all the samples possess MSE<10. Table .3 shows the ellipsometric data of as prepared SnO_2 samples. The thickness of the samples increases with molarity. Fig. 3(a) shows the change of thickness and roughness with doping concentration and Fig. 3(b) shows the variation of refractive index and extinction coefficient at 632.8 nm with concentration of precursor solution.

3.4. Optical properties

Fig. 4(a) shows the transmission spectrum of pristine SnO_2 thin films for different molarities of the precursor solution. Transmission percentage varies with molarity and all samples show constant transmission over the entire visible region. A maximum of about 60% transmission is observed for the film with 0.2 M concentration.

The determination of band gap is an important aspect to characterize the sample. Here Tauc plot is used to find the band gap using the relation proposed by Tauc, Davis and Mott [20].

$$\alpha h\upsilon = A\left(h\upsilon - E_g\right)^n \tag{4.5}$$

In the equation, hυ refers to the photon energy, α the absorbance, n = ½ for direct transition.

The optical band gap has been determined by extrapolating the linear portion of the $(\alpha h\upsilon)^2$ V hυ curve to x axis (Fig. 4(b)).

The band gap values vary from 3.26 to 3.75 eV for as prepared

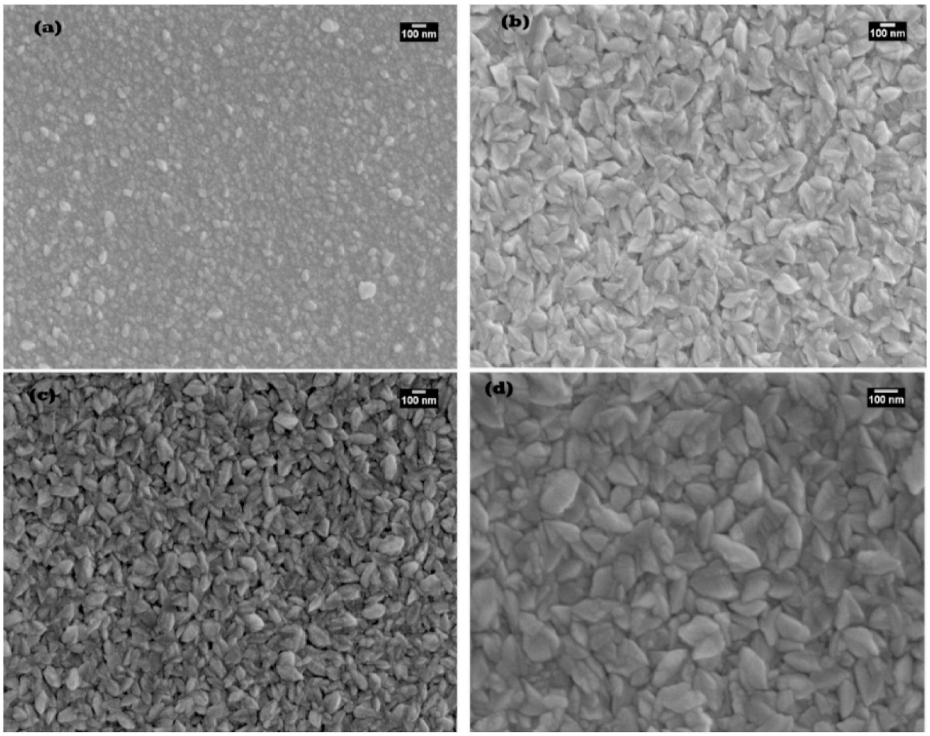

Fig. 2. SEM images of SnO_2 thin films for different precursor molarities (a) 0.05 M, (b) 0.15 M (c) 0.2 M and (d) 0.3 M.

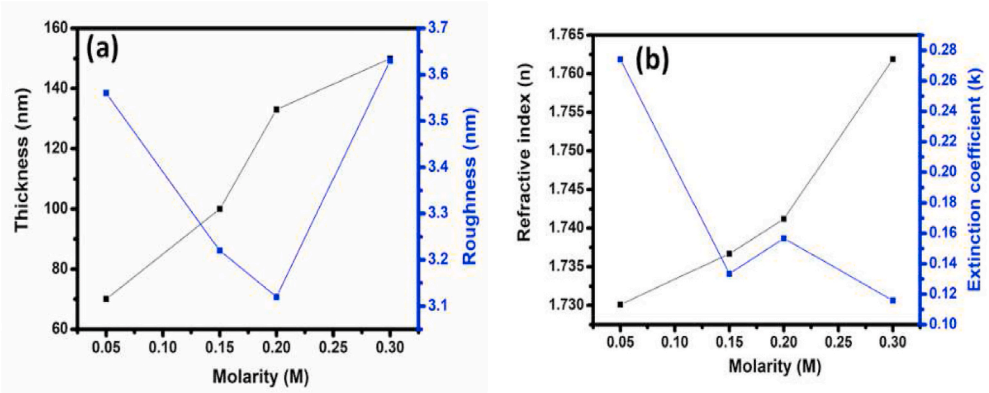

Fig. 3. (a) Variation of thickness and roughness of films with doping concentrations and (b) Variation of refractive index and extinction coefficient of films at 632.8 nm with doping concentration.

samples from various precursor concentrations. It can be observed that the band gap and carrier concentration are increasing with increase in precursor molarity as shown in Table 5. Blue shift in band gap when the carrier concentration is increased is due to Burstein-Moss effect according to which lower states of conduction band will be occupied by excess free electrons and electrons need additional energy to promote from valence band to conduction band. For the samples synthesized at 0.05 M and 0.15 M, the band gap is less than the bulk value (3.6 eV) showing band tailing effect. From Fig. 4(b) it is observed that the band gap increases with molarity.

Absorption spectrum of SnO_2 thin film samples for different precursor molarities is shown in Fig. 4(c). Absorbance increases smoothly with decrease in wavelength and exhibits a linear increase after the absorption edge. No absorption of light of sub band gap energy is noticed except for a slight distortion for 0.05 M and 0.15 M samples.

3.5. Photoluminescence (PL) studies

The photoluminescence (PL) spectra of the as grown samples are depicted in Fig. 5(a). Photoluminescence spectra of the samples are found to possess two broad emissions which corresponds to near band edge emission (NBE) and deep level emission (DLE) in the region 380–630 nm. Generally, NBE emission is due to excitons and DLE is due to intrinsic and extrinsic defects. The NBE and DLE emission peaks for 0.3 M sample are 410 nm and 528 nm respectively. It is observed that NBE emission intensity increases with molarity due to the increase in film thickness. A red shift in the NBE emission peak can also be observed due to the red shift in band gap with decrease in molarity of precursor solution.PL spectrum of optimised sample 0.2 M is deconvoluted and verified the presence of two emissions (Fig. 5(c)). For 0.05 M sample the two emissions merged to form an asymmetric broad emission.

The oxygen vacancies present in the samples act as luminescent centres. Oxygen vacancies can be neutral (Vo^0), singly charged (Vo^+) or doubly charged (Vo^{2+}) [21–23]. Of these charged states, Vo^0 is a shallow donor which lies near the conduction band. Under flat-band conditions most of the oxygen vacancies are likely in the Vo + state. The deep level emission at 528 nm observed for all the molarities of SnO_2 thin films in the present investigation is mainly due to singly charged oxygen vacancies. Intensity of this emission increases with molarity of precursor solution, reaches a maximum for 0.2 M sample and then decreases. This means that Vo^+ states are maximum for this sample. This can be ascertained with the observation of increase in carrier concentration with rise in molarity of precursor solution as oxygen vacancies contribute free electrons. For 0.3 M sample DLE intensity decreases even though carrier concentration is maximum. Here the increased carrier concentration may be due to doubly charged oxygen vacancies.

The chromatic coordinates (x, y) of the emission spectrum are calculated using the CIE coordinate calculator and represented in the CIE chromaticity diagram shown in Fig. 5(b). Table .4 shows the CIE coordinates of PL emissions from different samples.

Table 4
CIE coordinates of samples from various molarity of the precursor solution.

Molarity(M)	CIE Coordinates	Emission Colour
0.05	x = 0.278, y = 0.369	Green
0.15	x = 0.286, y = 0.365	Green
0.2	x = 0.273, y = 0.327	Bluish White
0.3	x = 0.297, y = 0.359	Greenish White

Table 5
Electrical characteristics of SnO_2 thin film samples.

Molarity (M)	Carrier concentration (/cm^3)	Resistivity (Ω cm)	Conductivity (S/cm)	Mobility (cm^2/V. s)	Band gap (eV)
0.05	$1.039x10^{19}$	$8.44x10^{-2}$	11.80	6.7	3.26
0.15	$2.061x10^{19}$	$4.51x10^{-2}$	22.20	7.1	3.55
0.2	$2.989x10^{19}$	$4.03x10^{-2}$	24.86	5.2	3.71
0.3	$3.012x10^{19}$	$4.34x10^{-2}$	23.03	4.7	3.75

3.6. Electrical studies

The electrical properties of samples are characterized at room temperature using Hall probe measurements in a Vander Pauw configuration. All SnO_2 thin film samples show n-type conduction due to the presence of oxygen vacancies. The mobility, hole concentration, and resistivity of the present samples are shown in Table 5.

It is observed that the carrier concentration increases with increasing molarity of the precursor solution. Increase in carrier concentration is due to increase in oxygen vacancy states in the SnO_2 thin films. Mobility shows a fluctuating behaviour which is due to the combined effect of increasing grain size and oxygen vacancies with increasing precursor molarity. An increase in grain size results in reduction in grain boundary scattering which leads to larger electron mobility. But vacancies act as defects which increases grain boundary scattering resulting in a decrease of electron mobility. Fig. 6(a) shows the change in conductivity and mobility with molarity of the precursor solution. The conductivity of the films increases with molarity up to 0.2 M and then decreases. This is in accordance with the variation in intensity of DLE emission in PL spectra.

It is appropriate to plot logarithm of the conductivity (ln σ) as a function of 1000/T for analysing the conductivity mechanism. Fig. 6(b) shows the Arrhenius plot of SnO_2 thin film samples from 0.2 M precursor solution for different temperatures in the range 308–423 K. From the figure it is clear that, all the samples show a semiconducting behaviour. The activation energy E_a is calculated from the slope of the Arrhenius plot [24]. The sample has two activation energies, one due to oxygen vacancies and the other due to intrinsic defects present in the films. The activation energies calculated are $E_{a1} = 0.0051$ eV and $E_{a2} = 0.0038$ eV.

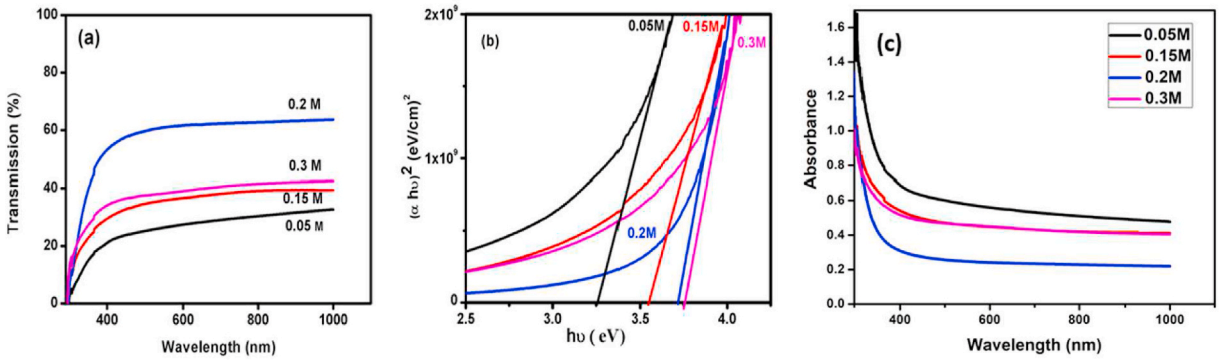

Fig. 4. (a) Transmission spectra, (b) Tauc plot and (c) absorption spectra of SnO_2 thin film samples for different precursor molarities.

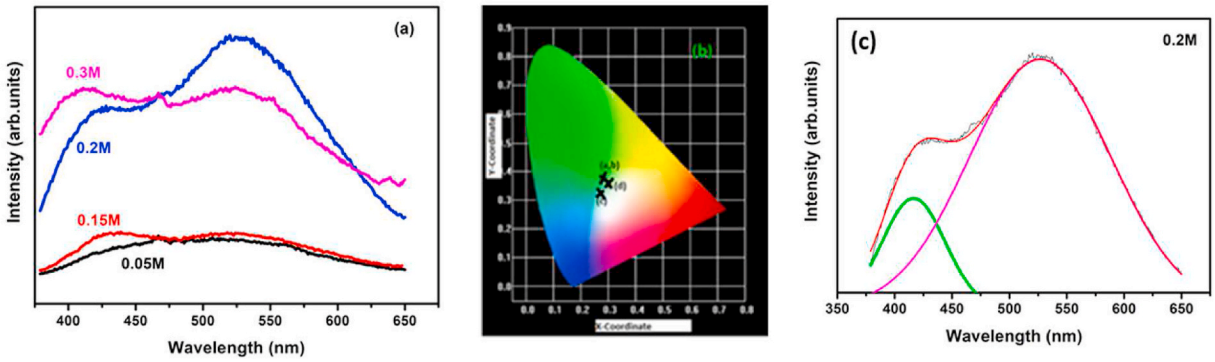

Fig. 5. (a) Photoluminescence spectra and (b) CIE diagram of SnO_2 thin films for different precursor molarities and (c) deconvoluted PL spectrum of 0.2 M sample.

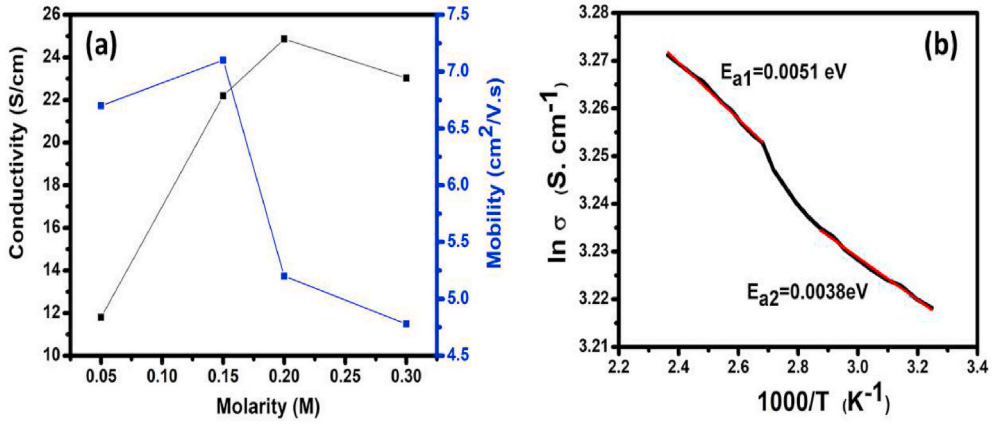

Fig. 6. (a). Variation of conductivity and mobility with molarity of precursor solution and (b) Arrhenius plot of SnO_2 thin film from 0.2 M precursor solution.

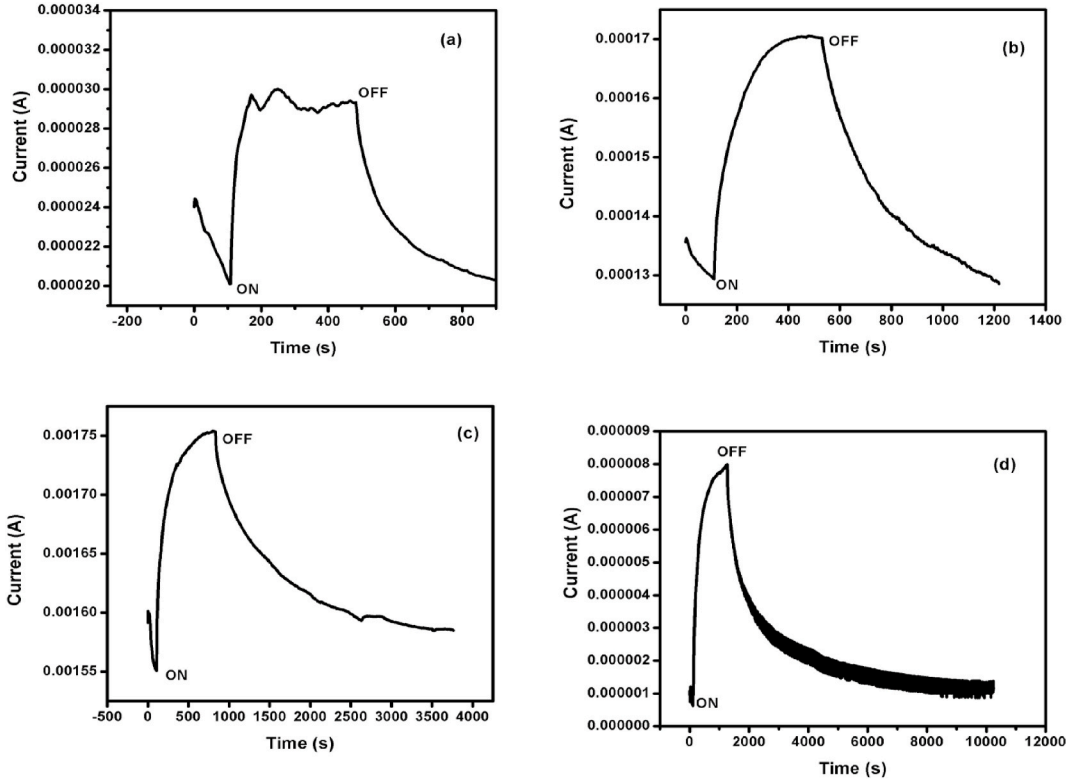

Fig. 7. Transient photoconductivity of as grown SnO_2 thin films for different molarities (a) 0.05 M, (b) 0.15 M, (c) 0.2 M and (d) 0.3 M.

3.7. Transient photoconductivity studies

To check the photo detector applicability of SnO_2 thin films, the samples were illuminated using halogen reflector lamp. All the synthesized SnO_2 thin films considered in the present study have photocurrent more than the dark current and hence show positive photoconductivity. This is due to the absorption of photons by mobile charge carriers present in the samples [25]. The time-resolved rise and decay of photocurrent spectra of as grown SnO_2 thin film samples for different molarities are shown in Fig. 7.

The dark current is measured upto 100s and then the sample is illuminated by Halogen reflector lamp. On illumination, the photocurrent initially increases in all the samples. This may be due to fast production of electron–hole pairs as a result of absorption of photons. The photocurrent decreases exponentially within few seconds after the illumination is switched off and attains a constant value after a long time. The decrease in the photocurrent is due to the recombination of electron-hole pairs with each other and captured by re-adsorbed oxygen molecules [26]. Even though all the samples have positive photoconductivity, it cannot be used for photo detector applications because it cannot have fast photo response. But it can be improved by suitable dopants on SnO_2 thin films.

4. Conclusions

Molarity of precursor solution affects the properties of SnO_2 thin film samples prepared by chemical spray pyrolysis method. Ellipsometric studies exposed the quality of films as good since all the samples possess MSE<10 and the sample prepared at 0.2 M concentration of precursor solution has minimum MSE and surface roughness values. Maximum transmission of 60% in the visible region, maximum conductivity of 24.86 S/cm and moderate mobility of 5.2 cm^2/V.s were shown by 0.2 M sample. The results suggest that SnO_2 thin film fabricated with 0.2 M precursor solution can be used as the n-layer in p-n junction diode.

CRediT authorship contribution statement

Ebitha Eqbal: Formal analysis, Investigation, Methodology, Validation, Writing – original draft, Writing – review & editing. **E.I. Anila:** Conceptualization, Funding acquisition, Investigation, Supervision, Validation, Writing – review & editing.

Declaration of competing interest

The authors declare that they have no known competing financial interests or personal relationships that could have appeared to influence the work reported in this paper.

Acknowledgements

Authors acknowledge the contribution of Dr.T L Remadevi in copy editing.

References

[1] M. Batzill, U. Diebold, Prog. Surf. Sci. 79 (2005) 47.
[2] A.L. Dawar, J.C. Joshi, J. Mater. Sci. 19 (1984) 1.
[3] J.B. Yoo, A.L. Fahrenbruch, R.H. Bube, J. Appl. Phys. 68 (1990) 4694.
[4] R.S. Rusu, G.I. Russia, J. Optoelectron. Adv. Mater. 7 (2) (2005) 823.
[5] M. Penza, S. Cozzi, M.A. Tagliente, L. Mirenghi, C. Martucci, A. Quirini, Thin Solid Films 71 (1999) 349.
[6] C. Li, M. Lv, J. Zuo, X. Huang, Sensors 15 (2015) 3789.
[7] R.E. Presley1, C.L. Munsee1, C.H. Park, D. Hong, J.F. Wager, D.A. Keszler, J. Phys. D Appl. Phys. 37 (2004) 2810.
[8] E. Elengovan, K. Ramamurthy, J. Optoelectron. Adv. Mater. 5 (1) (2003) 45.
[9] K. Kolentsov, L. Yourukova, A. Zheliaskova, A. Rachkava, Bulg. J. Phys. 31 (2004) 87.
[10] E. Manea, E. Budianu, M. Purica, C. Podaru, A. Popescu, I. Cernica, F. Babarada, C. C. Parvulescu, Rom. J. Inf. Sci. Technol. 10 (1) (2007) 25.
[11] S.I. Abbas, S.F. Hathot, A.S. Abbas, A.A. Salim, Opt. Mater. 117 (2021) 111212.
[12] P. Sivakumar, H.S. Akkera, T.R. K Reddy, Y. Bitla, V. Ganesh, P.M. Kumar, G. S. Reddy, M. Poloju, Opt. Mater. 113 (2021) 110845.
[13] K.S. Shamala, L.C.S. Murthy, N. Raok, Bull. Mater. Sci. 27 (3) (2004) 295.
[14] A.P. Caricato, A. Luches, R. Rella, Sensors 9 (2009) 2682.
[15] V. Kumar, A. Jain, D. Pratap, D.C. Agarwal, I. Sulaina, V.V. Sivakumar, A. Tripathi, S. Varma, R.S. Chauhan, Adv. Mat. Lett. 4 (6) (2013) 428.
[16] Ebitha Eqbal, E.I. Anila, Opt. Mater. 118 (2021) 111281.
[17] B.D. Cullity, Elements of X-Ray Diffraction, A. W. Pub. Comp. Inc., 1978, p. 99.
[18] G.K. Williamson, W.H. Hall, X-ray line broadening from filed aluminium and wolfram, Acta Metall. 1 (1953) 22.
[19] E. Benouis, M. Benhaliliba, F. Yakuphanoglu, A. Tiburcio Silver, M.S. Aida, A. Sanchez Juarez, Synth. Met. 161 (2011) 1509.
[20] T.A. Safeera, N. Johns, E.I. Anila, A.I. Martinez, P.V. Sreenivasan, R. Reshmi, M. Sudhanshu, M.K. Jayaraj, J. Anal. Appl. Pyrolysis 115 (2015) 96.
[21] F. Gu, S.F. Wang, M.K. Lu, X.F. Cheng, S.W. Liu, G.J. Zhou, D. Xu, D.R. Yuan, J. Cryst. Growth 262 (2004) 182.
[22] L.Z. Liu, X.L. Wu, J.Q. Xu, T.H. Li, J.C. Shen, P.K. Chu, Appl. Phys. Lett. 100 (2012) 121903.
[23] K. Vanheusden, W.L. Warren, C.H. Seager, D.R. Tallant, J.A. Voigt, B.E. Gnade, J. Appl. Phys. 79 (1996) 7983.
[24] S.M. Chou, L.G. Teoh, W.H. Lai, Y.H. Su, M.H. Hon, Sensors 6 (2006) 1420.
[25] F Moharrami, M.M. Bagheri-Mohagheghi, H Azimi-Juybari, Thin Solid Films 520 (21) (2012) 6503.
[26] Z.M. Liao, J. Xu, J.M. Zhang, D.P. Yu, Appl. Phys. Lett. 93 (2008), 023111.